Experimental Investigation of External Optical Injection and its Application in Gain-Switched Wavelength Tunable Optical Frequency Comb Generation

Gaurav Jain, Deseada Gutierrez-Pascual, Michael J. Wallace, John F. Donegan, *Senior Member, IEEE*, and Prince M. Anandarajah, *Senior Member, IEEE*

***Abstract*—A detailed experimental investigation of the effects of external optical injection on a Fabry Perot laser when in continuous wave (CW) mode and in gain switched mode is presented. Such detailed characterisation can help in optimising operating condition of the transmitters to significantly improve the system performance for dedicated applications. In CW mode, we characterised various performance indicators of a laser such as side mode suppression ratio (SMSR), wavelength, peak power, modulation bandwidth, resonance frequency, optical linewidth, and phase noise under external optical injection with the use of tuning maps. We also present in brief the theoretical origin of these parameters using rate equations. We then investigated the performance of the externally injected Fabry Perot laser under gain switching for optical frequency comb (OFC) generation. We demonstrated the generation of an OFC with a free spectral range of 6.25 GHz to 25 GHz and a quasi-continuous wavelength tunability of 31 nm. The phase noise of the tones of the generated OFC is measured and is found to be similar to that of the externally injected light and the measured optical linewidth was ∼40 kHz. We also presented experimentally the trade-off that exists between bandwidth of the generated OFC and the phase noise of individual comb tones under external optical injection and their optimisation for the application at hand.**

***Index Terms*—External optical injection, free spectral range, gain switching, linewidth, modulation bandwidth, optical frequency comb, phase noise, rate equations, resonance frequency, SMSR, wavelength tunability.**

Manuscript received March 2, 2021; revised May 19, 2021; accepted June 11, 2021. Date of publication June 23, 2021; date of current version September 18, 2021. This work was supported by Irish Research Council under Grant EBPPG/2015/237, by SME instrument phase 2 under Grant Agreement 881158, and by Science Foundation Ireland under Grants 15/IA/2854, 15/CDA/3640, 17/NSFC/4918, 12/RC/2276_P2, 18/EPSRC/3591, and 16/RI/3698. *(Corresponding author: Gaurav Jain.)*

Gaurav Jain was with the School of Physics, Trinity College Dublin, Ireland He is now with Pilot Photonics Ltd., Ireland (e-mail: jaing@tcd.ie).

Deseada Gutierrez-Pascual is with Pilot Photonics Ltd., Ireland (e-mail: desi@pilotphotonics.com).

Michael J.Wallace was with Pilot Photonics Ltd., Ireland and is now with Bright Photonics, Eindhoven, The Netherlands (e-mail: wallacmj@tcd.ie).

John F. Donegan is with the School of Physics and CRANN, Trinity College Dublin, Ireland (e-mail: jdonegan@tcd.ie).

Prince M. Anandarajah is with Photonics Systems and Sensing Laboratory, School of Electronic Engineering, Dublin City University, Ireland (e-mail: prince.anandarajah@dcu.ie).

Color versions of one or more figures in this article are available at https://doi.org/10.1109/JLT.2021.3091956.

Digital Object Identifier 10.1109/JLT.2021.3091956

I. Introduction

IN THE last two decades, network traffic has seen a significant increase due to the evolution of the information age. The unprecedented growth in the network traffic is continuously increasing the demand for bandwidth that thus far has been met by technologies such as dense wavelength division multiplexing (DWDM) and high order modulation formats. However, the current trend of system capacity and internet traffic suggests that in the next decade the system capacity will fall behind the internet traffic by a factor of ten without innovative solutions [1]. Continual industry innovation is needed to keep pace with rapidly increasing internet traffic. In order to keep meeting the demand for bandwidth, optical networks must evolve towards higher performance, throughput, spectral efficiency, and reduced power consumption [2], [3]. Often a lightwave system is characterized by its spectral efficiency, which is the information rate that can be transmitted over a given bandwidth or channel spacing. Currently, commercial systems incorporating DWDM utilise a channel spacing of 50 GHz and can support data rates of up to 100 Gb/s [4]. In order to achieve further spectral efficiency, 400 Gb/s and, 800 Gb/s and, 1 Tb/s transponders, employing high order spectrally efficient modulation techniques such as Nyquist-Wavelength Division Multiplexing (N-WDM) or coherent optical orthogonal frequency division multiplexing (CO-OFDM) have been proposed [5]. Recent experiments have achieved a record-high of 17.3 bit/s/Hz spectral efficiency transmission over 50 km using probabilistic shaping of polarization division multiplexing (PDM) 4096-QAM [6]. Such modulation techniques can operate at closer channel spacing with reduced or no guard bands. This can significantly improve the spectral efficiency by reducing/eliminating the guard bands. This calls for a flexible grid which can dynamically adjust its channel spacing to accommodate varying capacity and different reach requirements [7], [8].

Implementation of flexible/elastic optical network puts certain stringent requirements on the transmitter design including high power, high side mode suppression ratio (SMSR), low phase noise, high wavelength stability, flexible channel spacing, spectral flatness and high phase coherence. Conventional transceivers are realised by employing a bank of independent

semiconductor lasers. Such transceivers suffer from thermal-induced wavelength drift and require dedicated temperature control and wavelength lockers for wavelength stabilisation which significantly increases the power and cost budget. They also suffer from lack of phase correlation between the carriers which is not essential but can be useful in reducing the computational complexity of the digital signal processing (DSP) engine [9]. A flexible grid optical network can be efficiently realised by employing an optical frequency comb source (OFC) [10]. An OFC can be defined as a laser or laser subsystem, capable of generating multiple precisely spaced discrete optical carriers that share a strong phase correlation [10]. In addition, the inherently precise and stable frequency spacing of OFC enables the reduction of guard bands and thus improving the spectral efficiency of a lightwave communication system utilising advanced multicarrier modulation techniques. OFCs based on the external injection of gain switched laser diodes satisfies most of the attributes required from such transmitters and has generated a significant interest over the years [12], [13]. The suitability of this approach lies in its capability for monolithic integration [15], [16], free spectral range tunability [17], large central wavelength tunability [12] and simplicity. The inclusion of external optical injection improves the slave laser performance [34], typically in terms of mode selectivity [18], resonance peak and modulation bandwidth enhancement [19], [20], and especially noise reduction [21], [22], making such a comb source particularly attractive for coherent applications requiring low linewidth multi-carrier transmitters.

Most of the previous work on the OFC generation through gain switching were focused on optical external injection of single mode lasers [11], [14]. In this paper, we present a very detailed experimental investigation of the effects of optical injection on Fabry Perot laser when in continuous wave (CW) and in gain switched mode for the very first time to the best of our knowledge. In Section II of the paper, we experimentally characterise the vital parameters of the gain switched laser including wavelength, SMSR, power, modulation response, resonance frequency, linewidth, and phase noise under external optical injection. Such characterisation can then be used to precisely operate the laser subsystem based on master-slave configuration for the application at hand to attain optimum system performance. Section III of the paper illustrates the importance of injection locking in the generation of a wide OFC with multiple carriers sharing a very high degree of phase correlation. Section III also presents results on the free spectral range (FSR) and quasi-continuous wavelength tunablity of the generated OFC. We assess the quality of the generated comb lines through phase noise and linewidth measurements. Finally, the effect of external optical injection on the overall bandwidth and the phase noise of the OFC is discussed.

II. External Optical Injection

External optical injection entails the coupling of light from an optically isolated external laser source, usually named as the master laser, into the cavity of another laser known as the slave [19], [23], [24], [25], [34]. External optical injection, in an injection locking regime (described later), is known to improve certain output characteristics of the slave laser performance, typically in terms of mode selectivity, high SMSR, relaxation oscillation and modulation bandwidth enhancement, and noise reduction. In this section, we will present experimental verification of this along with some theoretical insights.

The dynamics of an injection-locked laser can be understood by the steady-state analysis of the rate equation of semiconductor lasers with optical injection. The standard optical injection locking (OIL) rate equations can be found in [19], [20], [23], [25]. Equation 1 qualitatively explains the locking condition of the slave laser. It describes the differential of the phase, namely, and is a formula for the emission frequency of the laser [20].

$$\frac{d\phi\left(t\right)}{dt}=\frac{\alpha}{2}\,g_o\left[N\left(t\right)-N_{th}\right]-\kappa\sqrt{\frac{S_{inj}}{S\left(t\right)}}\sin\left(\phi\left(t\right)\right)-\Delta\omega_{inj} \tag{1}$$

where *S(t)*, and *N(t)* are the slave laser's photon, and carrier number. $\phi(t)$ is the phase difference between the internal and injected field from the master. g_o, N_{th}, and α are the slave laser's differential gain, threshold carrier number, and linewidth enhancement factor. κ, S_{inj}, and $\Delta\omega_{inj}$ denotes the injection terms and stands for the coupling rate, injected photon number, and detuning frequency, respectively. The coupling rate is the rate at which the injected photons enter the cavity and distribute themselves along the cavity length. The detuning frequency, $\Delta\omega_{inj}$, is the difference between the master laser's frequency and slave laser's free running frequency (without injection): $\Delta\,\omega_{inj}=\omega_{master}\,-\omega_{fr}$.

In equation 1, the relative change in frequency induced by the resonance shift which is caused due to the reduction of the carrier number under injection is denoted by the first term on the right-hand side. The second term captures the shift caused due to the coupling between internal and injected fields. In steady state, when injection locking is achieved, $\frac{d\phi}{dt}=0$. This means that when the sum of the relative changes in frequency caused due to reduction of carrier number under optical injection (first term of equation 1) and the coupling between internal-injected fields (second term of equation 1) is equal to the detuned frequency, $\Delta\omega_{inj}$ (third term of equation 1), the slave laser is considered to be injection locked. This is the steady state solution of the equation 1. By substituting the steady state solution for various parameters in equation 1, and solving for the detuned frequency, we obtain:

$$\Delta\,\omega_{inj}=\frac{\alpha}{2}\,g_o\left[N_s-N_{th}\right]-\kappa\sqrt{\frac{S_{inj}}{S_s}}sin\left(\phi_s\right) \tag{2}$$

For a free running Fabry-Perot (FP) laser, the m^{th} longitudinal modes corresponding to the FP cavity resonance can be written as:

$$\omega_{fr}=\frac{mc}{2\mu l} \tag{3}$$

here, ω_{fr} is the free running frequency of the m^{th} longitudinal mode, c is the speed of light in vacuum, μ is the refractive index of the active layer and l is the cavity length. Equation 3 shows that the frequency of emission is inversely proportional

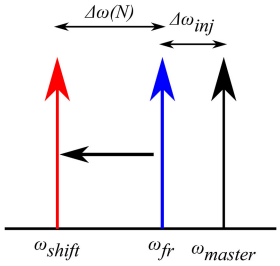

Fig. 1. Cavity resonant condition under injection locking.

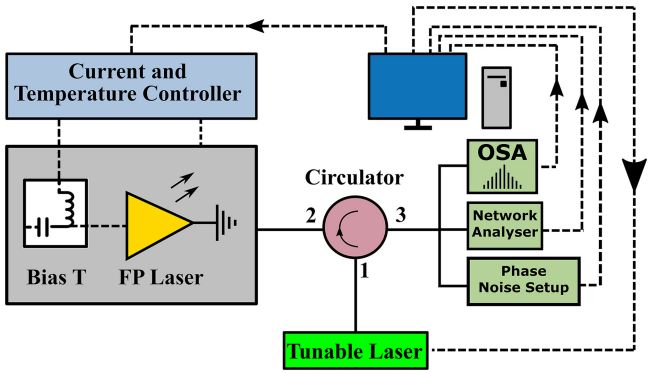

Fig. 2. Experimental setup to obtain locking maps of SMSR, peak wavelength, peak power, peak resonance, modulation bandwidth, and linewidth for various detuning and injected power.

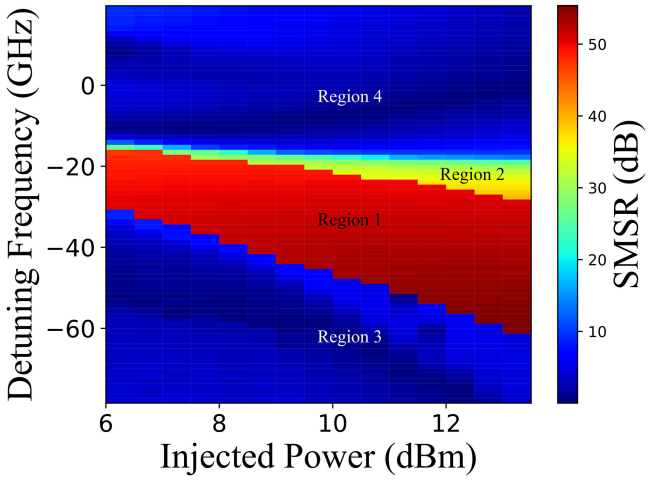

Fig. 3. Locking map showing steady state SMSR for the mentioned injected power and detuning.

to the refractive index of the laser material. Also, refractive index is a material property and shares an inversely proportional relationship with the carrier number, *N*, in the cavity. Hence, the increase (decrease) in the carrier number, increases (decreases) the emission frequency. This relationship can be expressed as [23]:

$$\Delta\omega\ (N) = \frac{\alpha}{2}\, g_o \Delta N \tag{4}$$

here, α is the linewidth enhancement factor, g_o is the differential gain, and $\Delta N = N - N_{th}$, N_{th} is the threshold carrier number. Fig. 1 considers the case of injection locking. Here, ω_{fr} is the free running frequency of the m^{th} longitudinal mode of the FP cavity resonance, and ω_{master} is the frequency of the injected field (master-laser). Due to the increased number of photons in the slave laser's cavity, the steady state carrier number goes below the threshold value, this redshift the cavity mode as per equation 4. This change is depicted in Fig. 1 by the frequency ω_{shift}. But under injection locking, the frequency of the output light is ω_{master}, not ω_{shift}. From Fig. 1, and equation 2, we can deduce that despite being injection locked, the slave laser continues to emit photons at a frequency which corresponds to its cavity resonance condition, ω_{shift}. Under injection locking, the injected master light continuously shifts the phase of the slave laser's light such that the slave laser's output appears to lase at the frequency of the injected light (master-laser). These phase-shifted photons undergo stimulated emission and creates more photons which are phase correlated to the new phase [19].

A. Experimental Set Up

Fig. 2 shows the experimental setup used to assess the effect of injection locking on the output characteristics of the slave laser. A Fabry Perot laser is used as the slave laser for this characterisation. The FP laser exhibited a threshold current of ∼10 mA at 20 °C. Detailed characterisation of this FP laser is included in section 3. The slave laser was biased at 26.3 mA and maintained at a temperature of 15.3 °C. The free running longitudinal mode at 1563.76 nm of the FP laser cavity resonance is selected to study the slave laser under optical injection. A low-linewidth semiconductor laser, wavelength tunable in the C-band is used as a master laser, injecting light in the cavity of the slave laser using a polarisation maintaining (PM) circulator. Both the slave and master lasers are pigtailed with PM fiber. The emission wavelength of the master laser is varied from 1563.6 nm to 1564.4 nm in steps of 0.01 nm to vary the detuning frequency, $\Delta\omega_{inj}$. Also, the emission power of the master laser is varied to emulate injection ratio variation. The output of the externally injected slave laser is then passed to an optical spectrum analyser (OSA – Yokagawa, AQ6370), a vector network analyser (VNA – Hewlett-Packard 8510C), and a phase noise setup for spectral, modulation response and phase noise measurements, respectively.

B. Spectral Characterisation

Fig. 3 shows the SMSR map of the slave laser under external optical injection. The vertical axis shows the optical frequency detuning between the master laser and the free-running slave laser (1563.78 nm), and the horizontal axis shows the injected master power in the cavity of slave laser. The main information extracted from Fig. 3 are the different operating regimes under external optical injection. Region-1 signifies a stable injection locking regime, which is the most important regime for all the major applications including direct modulation and coherent communications. Region-2 denotes the chaotic regime. In this region the oscillation undergoes amplitude and non-linear

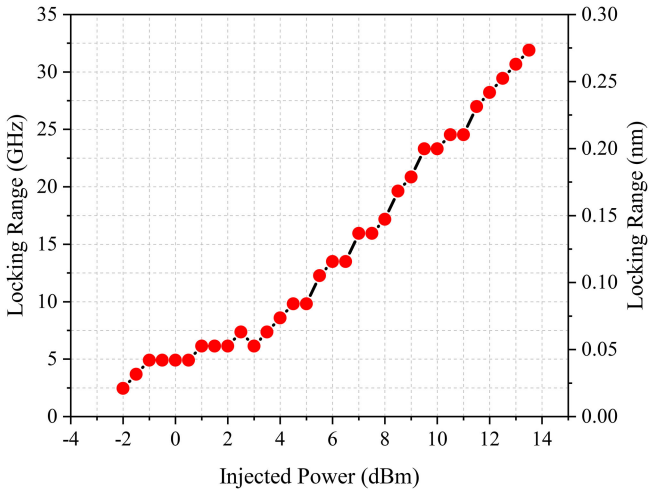

Fig. 4. Locking Range of the slave laser vs injected power from master laser.

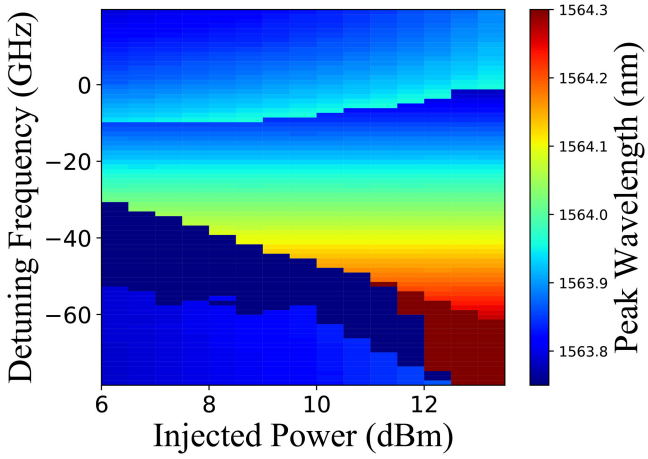

Fig. 5. Locking map showing steady state peak wavelength for the mentioned injected power and detuning.

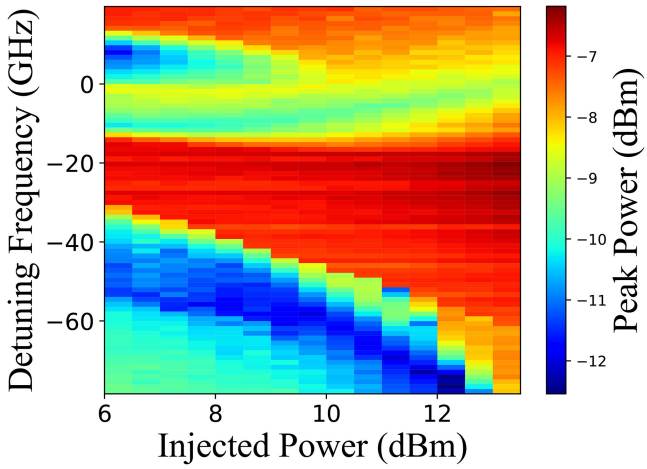

Fig. 6. Locking map showing steady state peak power for the mentioned injected power and detuning.

frequency modulation, which leads to a phenomenon like self-pulsation. Region-3, and Region-4 corresponds to the regime where four-wave mixing between internal and injected fields occur in the laser cavity. These non-linear effect in Region-23 and 4 have been extensively studied by many authors [26], [27], [28], [29]. In this work we mainly focus our attention on the stable injection locking regime (Region-1), as in this region we see the enhancement in various slave laser characteristics including modulation bandwidth enhancement and noise-reduction. In the rest of the paper, the injection locking regime will refer to the stable locking regime unless specified otherwise.

Fig. 3 shows that in the injection locking regime, all the longitudinal modes of the FP cavity are suppressed except for the one injection locked to the master laser, and the SMSR in this regime is ∼50 dB. The locking range is defined as the range of frequencies of the injected light from the master-laser at a given injected power into the cavity of the slave-laser over which the slave-laser is injection locked (dragged in frequency) to the injected light. This corresponds to a very good single mode performance with an SMSR in excess of 45 dB. The lock-in range in Fig. 3 is centered around −20 GHz instead of zero. This is due to the redshift of the slave laser wavelength under external optical injection. Due to the increased number of photons in the slave laser's cavity, the steady state carrier number goes below the threshold value, which redshifts the cavity mode as per equation 4. At low external optical injection where the locking-range is narrow, the master laser's wavelength has to be higher than the slave laser free running wavelength to be in the locking range for successful injection locking. In Fig. 4, the observed locking range for different levels of injection power, is plotted. It can be observed that the locking range increases with injected power within the given range of injected power. We have achieved a maximum 32.5 GHz of locking range at 13.5 dBm of optical injection.

Fig. 5 shows the corresponding output peak wavelength maps under external optical injection. As discussed earlier, even though the FP cavity resonance condition redshifts the slave laser's resonant cavity frequency under external optical injection, the output of the slave laser follows the master laser wavelength once injection locked. It can be clearly seen in Fig. 5, that the output wavelength from the slave laser follows the wavelength of the injected light in the region of injection locking.

Finally, the corresponding map for the peak power (power of the injected mode) is presented in Fig. 6. In a FP spectrum, the power gets distributed among many longitudinal modes. However, under injection locking, the single mode emission wins and captures most of the gain. As is clear, the peak power significantly improves under injection locking.

C. Enhancement of the Resonance Peak and Modulation Response

When the slave laser is injection-locked, it emits all the power at the injected frequency, ω_{master}. However, since the carrier number is reduced below its threshold value due to external optical injection, the cavity resonance condition redshifts as given by equation 4. As shown in Fig. 5, once locked, the

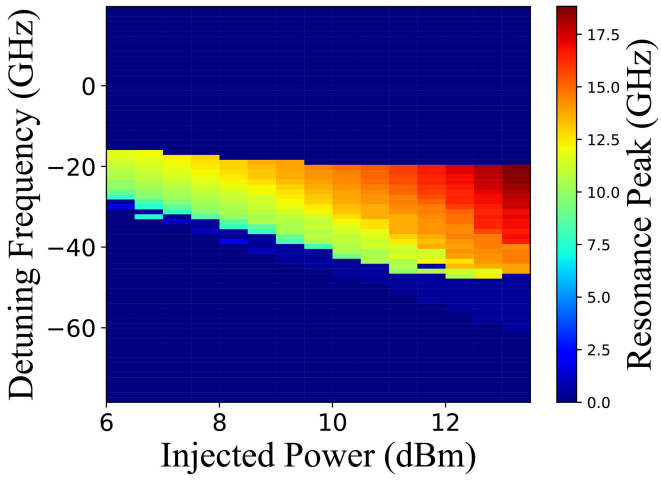

Fig. 7. Locking map showing the resonance peak for mentioned injected power and detuning.

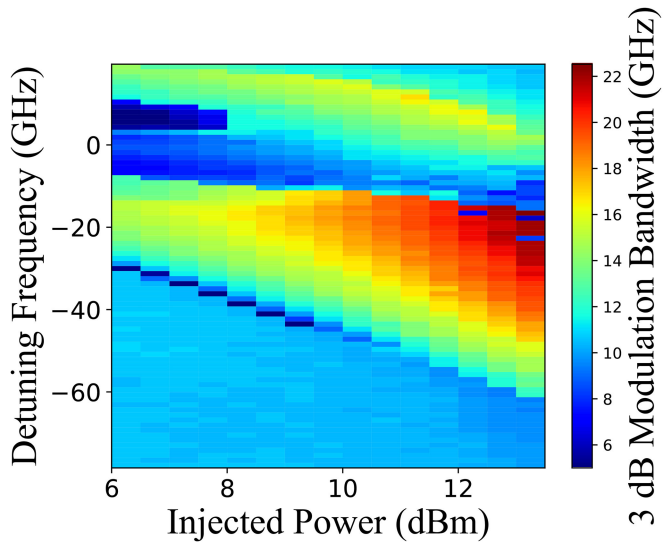

Fig. 8. Locking map showing the 3 dB modulation bandwidth for mentioned injected power and detuning.

slave laser lases at ω_{master} and not at its cavity resonance condition, ω_{shift}. This frequency detuning between the cavity resonance condition, ω_{shift} , and the lasing wavelength, ω_{master}, influences the modulation response [26] and results in the resonance frequency enhancement [19]. In [20], the authors have shown that during the transient processes, the field corresponding to the cavity resonance condition is generated. This field then interferes with the injection locked field. Due to this interference, the output laser intensity exhibits a beat at the detuned frequency. Such transient field diminishes in the steady state, as all the optical gain is provided to the locked field. The enhanced resonance frequency ($\Delta\omega_{res}$) produced by this interaction can be given by the difference between injected field frequency, ω_{master}, and the cavity resonance condition, ω_{shift}: $\Delta\omega_{res} = \omega_{master} - \omega_{shift}$. From Fig. 1, and equation 4, this can be further written as:

$$\Delta\,\omega_{res} = \Delta\omega_{inj} - \frac{\alpha}{2} g_o \Delta N \tag{5}$$

Then according to [19], the resonance frequency (ω_{res}) can be written as equation 6. Here, $\omega_{res,0}$ is the resonance frequency of the free running slave laser.

$$\omega_{res}^2 \sim \omega_{res,0}^2 + \Delta\omega_{res}^2 \tag{6}$$

The modulation response and resonance frequency of the slave laser under external optical injection is measured using a Vector Network Analyser (VNA). The free running modulation response of the slave laser at various currents is shown in Fig. 13(c). Fig. 7 shows the corresponding maps of resonance frequency of the slave laser under optical injection. The resonance frequency of the slave laser under external optical injection is measured by locating the peak of the modulation response curve. The maps show 2 profound variations:

- ***Frequency of resonance increases with injected power:*** This variation can be easily understood from equation 5 and 6. For a given detuning, as the injected power in the slave laser cavity increases, the carrier number decreases. This reduction in carrier number further redshifts the cavity mode, ω_{shift}, as given by equation 4. This increases the detuning between the injected frequency, ω_{master} and the cavity mode, ω_{shift} and results in the increment of the resonance frequency, ω_{res}.
- ***Frequency of resonance increases (decreases) with positive (negative) detuning:*** For increasingly negative detuning frequencies, the master laser frequency approaches the cavity mode (see Fig. 1) and the resonance frequency enhancement decreases. However, for a positive detuning, the master moves in the opposite direction of the cavity mode migration, creating larger resonance frequency enhancements, with the largest enhancement occurring at the positive edge of the locking range.

The 3 dB modulation bandwidth of the slave shows a similar pattern as the resonance frequency and the corresponding maps of the slave laser's 3 dB modulation bandwidth under external optical injection is presented in Fig. 8. One important point to notice here is that the modulation bandwidth of the slave laser is enhanced from its intrinsic value of ∼6 GHz to ∼22 GHz for the given injection parameters. This large improvement in the modulation response of the slave laser is a direct consequence of external optical injection.

D. Noise Reduction

The phase noise of a semiconductor laser diode is an important parameter in coherent communication systems. For such systems, the phase noise requirements of the optical transmitter become very stringent [36]. In this work, the noise in the optical signal is characterised by measuring the frequency modulated (FM) - noise spectrum, which fully describes the noise processes contributing to the overall phase noise [30]. The optical linewidth is then calculated through the flat white noise component of the FM-noise spectrum.

The experimental characterisation of the FM-noise spectrum is performed via a phase noise measurement method previously

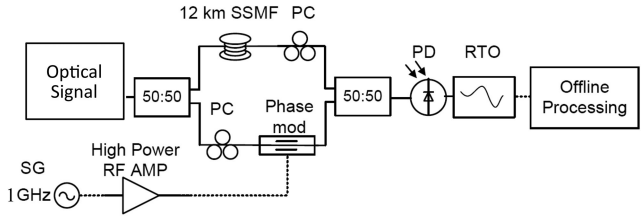

Fig. 9. Experimental set up for phase noise measurements using the modified delayed self-heterodyne detection method. SSMF: standard single mode fiber; PC: polarization controller; SG: signal generator; RF AMP: RF amplifier; Phase mod: phase modulator.

developed [30], whose set up is presented in Fig. 9. The technique used here to measure the phase noise of the optical signal is based on the technique presented in [30] and is commonly known as the modified delayed self-heterodyne. The optical signal to be measured is split into two equal parts using a 50:50 coupler. One part is de-correlated from the original/other signal by propagating it via 12 km of standard single mode fiber (SSMF). The other part is phase modulated, using a phase modulator driven by a high power 1 GHz signal to achieve second order harmonics. The light from both the arms are then recombined using another 50:50 coupler. The recombined signal is then passed to a photodetector. The detected heterodyne signal will present copies of doubled linewidth at 1 GHz harmonics, which are sampled and captured with the aid of a real time oscilloscope. The differential phase information is then recovered offline by following the procedure presented in [30]. Phase noise can be quantified by the power spectral density (PSD) of the differential phase, $S_{\Delta\phi_n}(f)$, having units of *rad²/Hz*. Phase noise is directly related to the frequency noise, as the instantaneous frequency, f_{ins}, is basically the time derivative of the phase, $\phi_n(t)$:

$$f_{ins} = \frac{1}{2\pi}\frac{d\phi_n(t)}{dt} \tag{7}$$

The PSD of the instantaneous noise frequency, $S_F(f)$, can be found from the PSD of differential phase, $S_{\Delta\phi_n}(f)$, using equation 8 [31]:

$$S_F(f) = \left(\frac{f}{2\sin(\pi f T)}\right)^2 S_{\Delta\phi_n}(f) \tag{8}$$

here, T is the time delay in the 12 km of SSMF. Now, for the white FM-noise, the single-sided PSD of the noise frequency can be written as:

$$S_F(f) = \frac{\delta f}{\pi} = S_0 \tag{9}$$

This leads to a double-sided field spectrum, *S(f)*, having the Lorentzian shape [31]:

$$S(f) = \frac{\delta f}{2\pi\left[f^2 + \frac{\delta f}{2}^2\right]} \tag{10}$$

Thus δf in equation 9 represents the full width at half maximum (FWHM) of the field spectrum (optical spectra). Hence the linewidth can be extracted from the flat portion of the

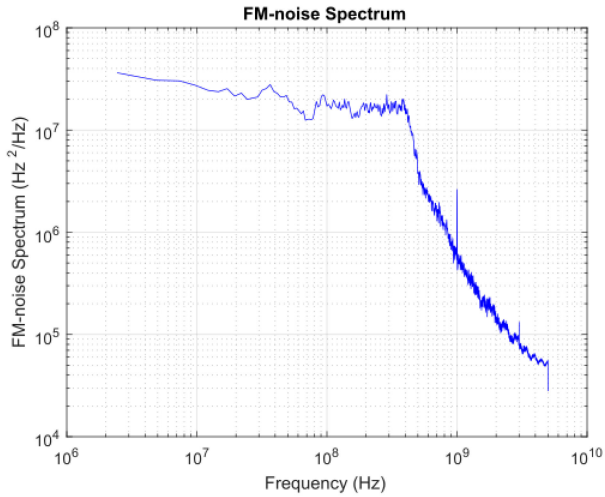

(a)

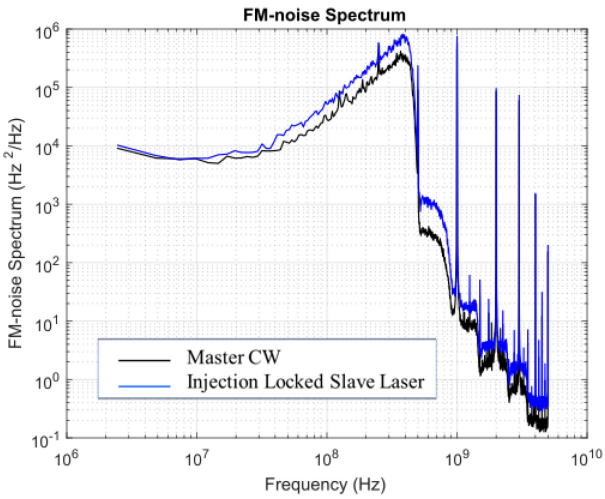

(b)

Fig. 10. Measured FM-noise spectrum of (a) Free running slave laser, and (b) master laser, and injection locked slave laser.

FM-noise spectrum (PSD of instantaneous noise frequency). In our measurement, the linewidth extracted from the FM-noise spectra plot is given by - FWHM $= \frac{\pi}{2}S_0$. The factor of 2 is added since the local oscillator light output and the signal are equally noisy.

In order to measure the FM-noise spectrum of the slave laser, the mode at 1563.78 nm of the FP laser was first filtered using a tunable optical filter with adjustable bandwidth, Yenista XTM-50. Fig. 10(a) shows the FM-noise spectrum of the slave laser which appears to be completely flat because its resonance peak lies far outside the observed frequency range. The measured linewidth from the flat white FM-noise component of the slave laser is of the order of tens of megahertz. Such a large linewidth makes the usability of higher modulation format challenging if not completely redundant (Baud rate dependant). Optical injection has been studied over many years, and has been shown to improve the noise characteristics of the injected laser [21], [22]. Injection from a high spectral purity master laser under optimised injection conditions can lead to the generation of

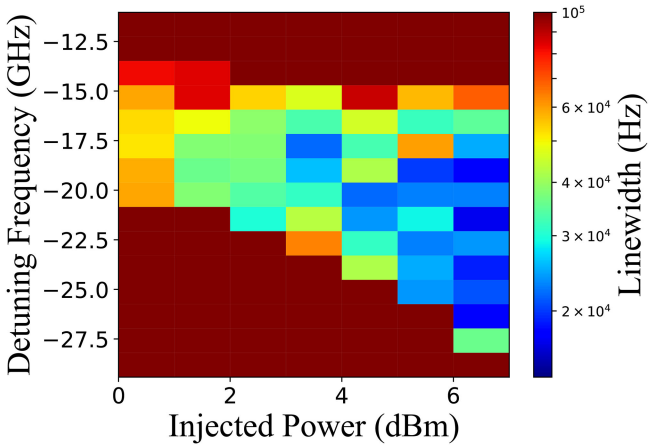

Fig. 11. Locking map showing the optical linewidth for mentioned detuning and injection ratio.

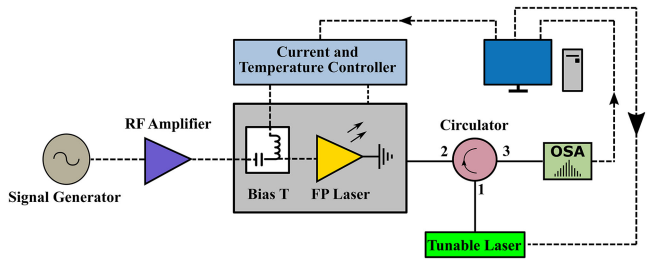

Fig. 12. Schematic diagram of the experimental set-up used to generate Gain-Switched Optical Frequency Comb (GS-OFC).

highly coherent output, equivalent to the master laser itself. Fig. 10(b) shows the FM-noise spectrum of the master laser (black). The measured linewidth from the flat white FM-noise component is ∼20 kHz. Fig. 10(b) also shows the FM-noise spectrum of the slave laser under external optical injection, with master laser operating at a detuning of −20.8 GHz and the injected power was 7 dBm. As expected, the external optical injection resulted in a superior performance in terms of noise. The FM-noise spectrum of the injected slave laser is equivalent to the master laser with a measured linewidth of ∼20 kHz.

Fig. 11 plots the linewidth map of the slave laser under external injection for the given detuning and injected power. As evident from the linewidth map, a linewidth of less than 60 kHz is obtained for all the points within the locking range. Also, as predicted in [22], for a given detuning, the laser linewidth continuously improves with the increased injected power. Also, the laser linewidth improves with negative detuning as predicted in [22].

III. Externally Injected Gain Switched Optical Frequency Comb

A. Experimental Set Up and DC Characterisation

The schematic diagram of the experimental set-up used to generate the gain switched optical frequency comb (GS OFC) is presented in Fig. 12. The slave laser used is a commercially sourced FP laser from Fraunhofer Heinrich Hertz Institute. This

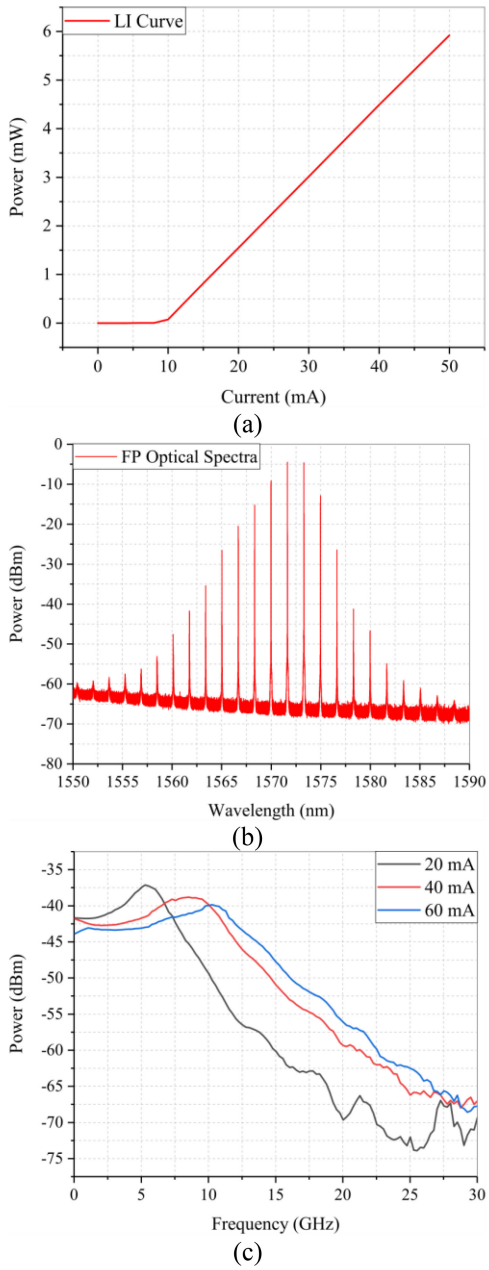

Fig. 13. FP laser CW characterization at 20 °C: (a) LI curve, (b) Optical spectrum at 50 mA, and (c) small-signal modulation response at 20, 40 and 60 mA.

device is packaged in an optically un-isolated and temperature controlled high-speed butterfly package. The P-contact of the laser diode is wire-bonded to the RF connector through an internal 47 Ω sheet resistor for impedance matching. The RF connection to the laser was designed to provide reasonable performance up to 40 GHz. The packaged device contains a 10 kΩ thermistor and a thermoelectric cooler (TEC) for sensing, controlling and stabilising the laser diode temperature. The optical light from the FP laser is collected using a PM fiber. As shown in Fig. 13(a), the FP laser exhibited a threshold current of ∼10 mA at 20 °C. The output emission of the FP laser falls within the C and L band with the emission peak around 1572.5 nm when

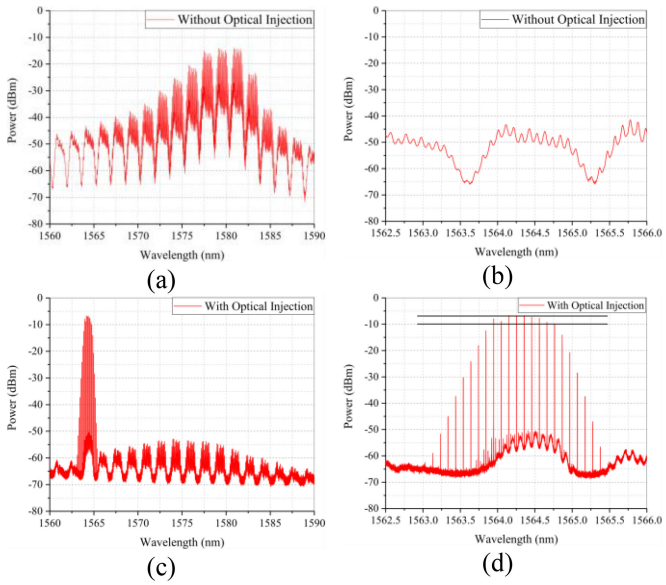

Fig. 14. Optical spectra of gain switched optical frequency comb at a gain switching frequency of 12.5 GHz: (a) without external injection, (b) without external injection, focusing on the non-dominating mode of the FP laser, (c) with optical injection, showing the excellent mode selectivity, and (d) with optical injection, focusing on the generated optical frequency comb with 9 lines in the 3 dB bandwidth.

biased at 50 mA at 20 °C, as shown in Fig. 13(b). The small signal modulation response of the FP laser at 20, 40 and 60 mA of injection current is recorded in Fig. 13(c). We observed a relaxation oscillation frequency of 5, 9 and 10 GHz at 20, 40, and 60 mA of bias current respectively. The observed small signal 3 dB modulation bandwidth at 60 mA of injection current is ∼13 GHz. A low linewidth tunable laser is used as a master laser to provide external injection through a PM circulator. The effect of optical injection on the output characteristics of the slave laser has already been characterised in detail and presented in the previous sections.

An external bias tee with a bandwidth of 26 GHz, is used to provide the DC bias and the gain switching signal to the slave laser as shown in Fig. 12. A Thorlabs LDC205C laser diode controller is used to provide the DC bias to the slave laser. Gain switching is achieved by applying an amplified RF sinusoidal signal (∼24 dBm) to the high-speed K connector of the bias tee. The RF sinusoidal signal was provided by a Rhode and Schwarz SMR40 signal generator and amplified by a HP 83020A RF amplifier. The output optical signal of the injected and gain-switched FP laser is then transferred to a high resolution (20 MHz/0.16 pm) OSA (Apex Technologies AP2083A), for spectral measurements.

B. Generation of GS-OFC with External Optical Injection

Fig. 14(a) shows the optical spectrum of the FP laser gain switched at a repetition rate of 12.5 GHz without external injection. As expected, due to lack of any mode selectivity, all the longitudinal modes of the FP laser are present in the optical output. The application of a large sinusoidal signal (∼24 dBm) resulted in the generation of an optical frequency comb at some

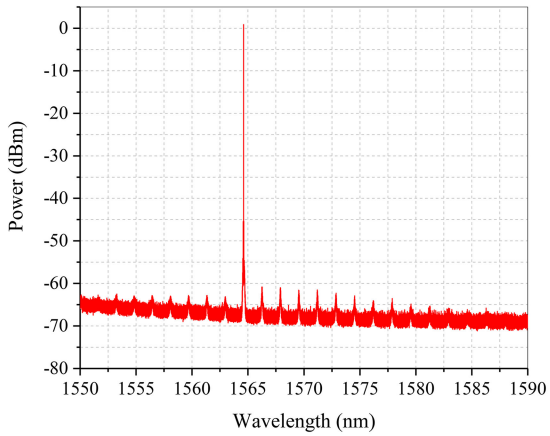

Fig. 15. Injection locked master-slave laser, showing excellent mode selectivity with an SMSR of $>$ 60 dB.

of the longitudinal modes (modes with higher power) and broadening of the others (modes with lower power). The applied gain switching signal drove the FP laser above and below threshold continuously which resulted in a high level of chirp and temporal jitter due to the poor phase correlation between consecutive pulses. Due to the lack of optical injection, the effects of mode partition noise (associated with FP laser) would manifest if such a signal was to transmit over fiber. As shown in Fig. 14(a), the OFC generated is a multimoded spectrum which is unusable due to inter-modal dispersion. The OFC generated at the dominating longitudinal modes of the FP cavity showed very poor spectral flatness and a carrier to noise ratio of $<$30 dB was observed for all the modes. The latter two ill-effects can be attributed to the lack of phase coherence between the consecutive pulses [37]. Fig. 14(b) focuses on the extreme modes of the optical output of Fig. 14(a), further away from the gain peak of the FP laser. In contrast to the dominating modes, gain switching of the extreme modes resulted in a significantly broadened spectrum with no discernible comb tones. All these factors make such a system practically inefficient/useless for all communication applications.

The challenges mentioned above can be mitigated by employing optical injection. Optical injection has been earlier shown to suppress the mode partition noise [18] to provide single mode performance with high SMSR [19], [23] and enhanced modulation bandwidth [19], [23], [32], [33].

Fig. 15 illustrates the mode-selectivity obtained through optimised optical injection. By applying optical {injection from the master laser into the cavity of the FP laser at 1564.6 nm, single mode performance with a SMSR $>$60 dB is obtained. Application of gain switching signal at 12.5 GHz to the slave laser at these operating points resulted in the generation of highly coherent frequency combs as shown in Fig. 14(c) and 14(d). The generated OFC at a free spectral range of 12.5 GHz showed very good flatness with a full width at half maximum of around 0.8 nm, having 9 comb tones within a 3 dB spectral ripple.

An SMSR and carrier to noise ratio (CNR) of more than 40 dB is also achieved. This indicates excellent pulse-to-pulse phase stability, phase correlation of the emitted pulses, and a

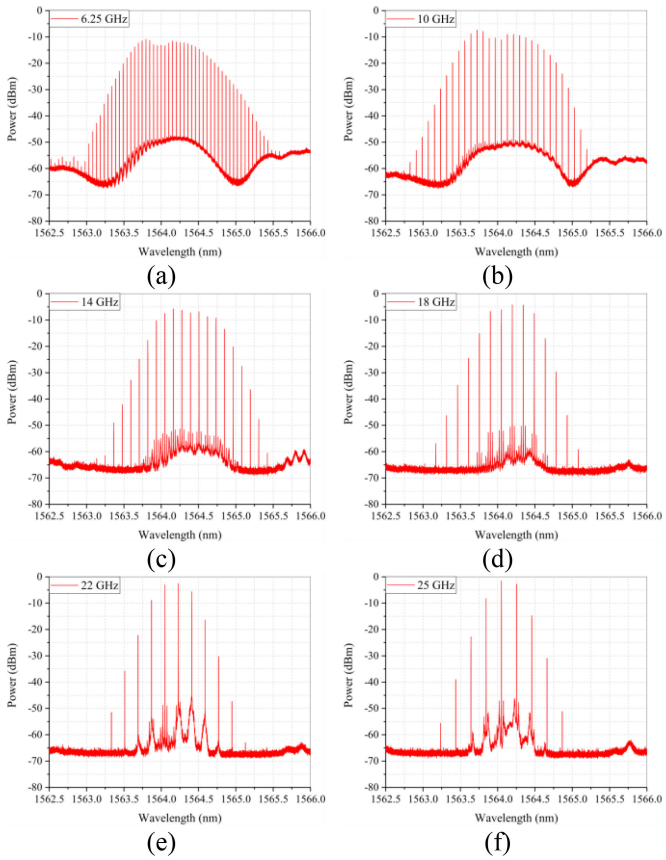

Fig. 16. Optical spectra of the GS-OFC generated with different FSRs: (a) 6.25 GHz, (b) 10 GHz, (c) 14 GHz, (d) 18 GHz, (e) 22 GHz, and (f) 25 GHz.

considerable reduction in the linewidth [35], [37]. Each of these generated frequency tones can be treated as an independent channel for data transmission, which removes the requirement of separate laser transmitters. These generated channels can then be separated using an optical demultiplexer. This reduces the cost of implementing a multicarrier transmitter substantially as this would not require multiple lasers, temperature controllers and corresponding wavelength lockers.

C. FSR Tunability

One of the major advantages of the GS-OFC apart from its simplicity, cost-efficiency, and stability, is its ability to achieve FSR tunability only restricted by the device's modulation bandwidth which can be significantly enhanced by optical injection. Since, in a GS-OFC, the frequency spacing between adjacent comb tones is set by the frequency of the applied radio frequency (RF) signal, precise and flexible FSR can be easily achieved.

Fig. 16 reports the generated GS-OFC with an FSR ranging from 6.25 to 25 GHz. Gain switching at these frequencies resulted in the generation of the OFC with 2-17 clearly discernible and phase correlated comb tones in the 3 dB bandwidth. A carrier to noise ratio of > 40 dB is observed for all the generated tones of the OFC. These results are obtained under the application of external injection from the master laser at 1564.05 nm.

TABLE I
OPERATING CONDITIONS FOR THE OFCS GENERATED AT VARIOUS FSRS IN FIG. 16

Free Spectral Range (GHz)	Master Laser Power (dBm)	Master Laser Wavelength (nm)	Slave Laser Bias Current (mA)	Slave Laser Temp. (°C)
6.25	6	1564.05	41.72	14.3
10	8	1564.05	49.19	16
14	10	1564.05	48.6	19.9
18	13.5	1564.05	48.6	19.9
22	13.5	1564.05	48.6	19.9
25	13.5	1564.05	49.58	21.5

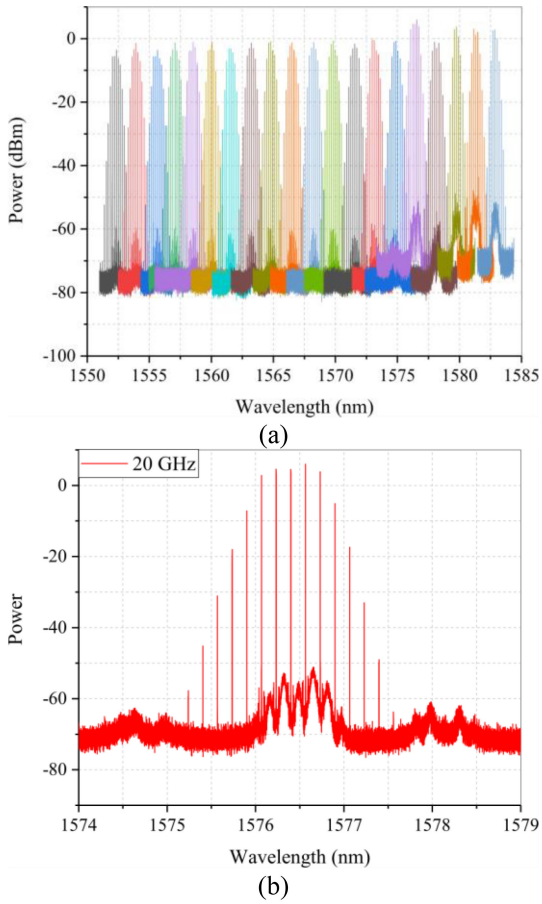

Fig. 17. Optical spectra of (a) overlapped GS-OFC with an FSR = 20 GHz covering wavelength range from 1552 nm to 1583 nm, and (b) GS-OFC with an FSR = 20 GHz with a central wavelength around 1576.5 nm having 5 lines in the 3 dB bandwidth.

The intensity of applied optical injection was varied from 6 to 13.5 dBm to keep the frequency of the relaxation oscillation close to the required FSR value, this resulted in the generation of an optimised comb with low temporal jitter [13]. Detailed operating parameters for generating these combs is presented in Table I.

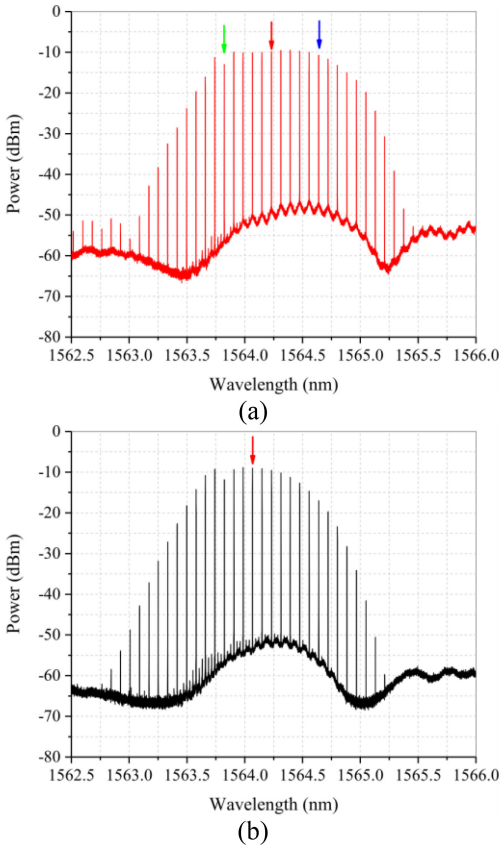

Fig. 18. Optical spectra of GS-OFC with external optical injection optimized for (a) flatness, and (b) low noise.

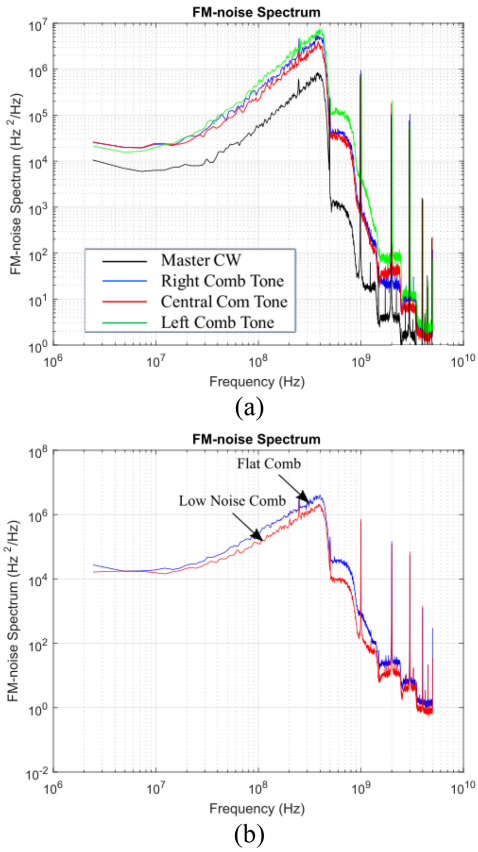

Fig. 19. Measured FM-noise spectrum for (a) master laser and the 3 comb tones marked in Fig. 18 (a), and (b) comparison of the phase of the central comb tone of the 2 combs shown in Fig. 18 (marked with red arrow).

D. Wavelength Tunability

As shown in Fig. 15, precise injection into a particular FP mode results into a single mode with an SMSR in excess of 60 dB. So, by carefully injecting into different FP modes which are separated by 1.66 nm (see Fig. 13(b)), a single mode operation on all the longitudinal modes of the FP laser can be achieved. Gain-switching at these operating points results in the generation of highly coherent optical frequency combs. In Fig. 17(a), the overlapped spectra of these generated OFC under a 20 GHz applied gain-switching signal is plotted, showing a quasi-continuous wavelength tuning from 1552 nm to 1583 nm, covering 31 nm. By carefully designing the FP laser, this wavelength span can be moved to the C-band or any other band of interest. The generated OFC on all the longitudinal modes consists of 5 clearly resolved comb tones separated by 20 GHz, one such OFC is shown in Fig. 17(b). Furthermore, finer wavelength tunability can be achieved by temperature tuning the slave laser and then carefully injecting into the desired FP mode.

E. Phase Noise

As mentioned earlier, the experimental characterisation of the FM-noise spectrum is performed using a phase noise method developed in [30]. The experimental setup is the same as presented in Fig. 9. In this case, the optical signal (GS-OFC) is passed through a narrow optical band pass filter (OBPF) that selects the individual comb line. Then the filtered comb line is passed through an Erbium doped fiber amplifier (EDFA) in order to compensate for the losses in the OBPF. The EDFA was set to amplify the input light to 3 dBm. The amplified optical signal was then passed to the modified-DSH setup for phase characterisation.

Fig. 18(a), shows the generated GS-OFC under external optical injection with an FSR of 10 GHz, for phase noise analysis. In this case the master laser was set at 13.5 dBm with emission at 1564.05 nm and the slave laser was biased at 48.4 mA at 20.5 °C. The phase noise measurement is carried on the marked comb lines in Fig. 18(a). These measurements are then compared with the phase noise characteristic of the master laser at those specific wavelengths. As shown in Fig. 19(a), the FM-noise spectrum of the master laser is dominated by the flat white FM-noise component which corresponds to a linewidth value of 20 kHz.

The filtered comb lines at each wavelength have similar FM-noise spectrum as the master at lower frequencies, as shown in Fig. 19(a). The corresponding linewidth for all the filtered comb tones is observed to be ∼40 kHz. At high frequencies the phase noise of the filtered comb lines presents an acceptable deviation from the master laser. This deviation was studied in [35] and is a consequence of residual phase noise from the slave laser, which depends on the injection parameters used (injected power and wavelength detuning). As pointed out earlier and

illustrated in Fig. 8, and 11, with negative (positive) detuning, the modulation response decreases (increases), and linewidth also decreases (increases). Hence, the noise in the optical comb lines can be further improved by negatively detuning the master - slave laser. But this leads to a reduced modulation response which reduces the overall flatness and 3 dB bandwidth of the comb. So there exists a trade-off between the phase-noise at higher frequencies and overall flatness of the comb. Hence the injection parameters should be chosen wisely according to the application at hand.

Fig. 18(b) shows a generated GS-OFC under external injection and with an FSR of 10 GHz. The slave laser was negatively detuned (by decreasing the operating temperature of slave laser to 19.2 °C) relative to master. As pointed out earlier, this resulted in a reduced modulation response and hence, a relatively narrower and not a flat comb compared to the one in Fig. 18(a). Fig. 19(b) compares the phase noise of the central comb lines (marked by red arrow in Fig. 18(a), and (b)) in these two cases. The 2 filtered comb lines have an almost identical FM-noise spectrum at lower frequencies. The comb line with increased negative detuning shows lower phase noise at higher frequencies as expected from the discussion earlier and as pointed out in [35].

From the results presented in Figs 19(a), and (b), the deviation in the FM-noise spectrum is acceptable hence suggesting optimum injection parameters for the generated GS-OFC. These results indicate that the comb tones would impose small penalties (compared to the master) when being employed in a coherent communication system [35].

IV. Conclusion

Networks incorporating flexible channel spacing to maximise the spectral efficiency by adapting to the demand of the network are gaining a lot of attention recently. Implementation of such networks calls for specialised transmitters capable of generating number of carriers, with high flatness, flexible channel-spacing, wavelength tunability, high SMSR, low-noise and cost and power efficiency. Currently, transmitters based on a bank of independent lasers are used. Such systems require a dedicated temperature control for wavelength stabilisation along with a large inventory which increases the power and overall cost budget. In this paper, we presented an innovative multicarrier transmitter, gain switched optical frequency comb (GS-OFC) utilising external optical injection, which can play a vital role in the implementation of flexible networks. We also provide a detailed experimental study of external optical injection by providing experimental verification of various benefits reaped from optical injection including single mode performance with high SMSR, wavelength stabilisation, resonance frequency, modulation response enhancement and noise reduction with the help of tuning maps. We presented a theoretical background as well to understand the origin of such enhancements. We then studied the performance of GS-OFC which takes the advantage of external optical injection to generate an OFC with clear multiple discernible comb tones with very high spectral purity, equivalent to the injecting laser (master). The spacing between the generated comb tones is governed by the frequency of the applied high power RF signal - this provides a huge range of FSR achievable. We presented a complete characterisation of the generated OFC including FSR tunability from 6.25 GHz to 25 GHz, wavelength tunability covering 31 nm, and low linewidth 40 kHz, and a carrier to noise ratio of $>$ 40 dB. We also studied experimentally the trade-off that exists between bandwidth of the generated OFC and the phase noise of individual comb tones under external optical injection, and demonstrated the optimisation of the OFC according to the application at hand. The presented GS-OFC employing external optical injection satisfies most of parameters required from the flexible networks and can prove critical in the implementation of such systems.

References

[1] R. Essiambre and R. W. Tkach, "Capacity trends and limits of optical communication networks," *Proc. IEEE*, vol. 100, pp. 1035–1055, May 2012.

[2] S. Gringeri, E. B. Basch, and T. J. Xia, "Technical considerations for supporting data rates beyond 100 gb/s," *IEEE Commun. Mag.*, vol. 50, pp. s21–s30, Feb. 2012.

[3] A. A. M. Saleh and J. M. Simmons, "Technology and architecture to enable the explosive growth of the internet," *IEEE Commun. Mag.*, vol. 49, pp. 126–132, Jan. 2011.

[4] B. Gowan, "Coherent optical turns 10: Here's how it was made," Mar. 2018. [Online]. Available: https://www.ciena.com/insights/articles/Coherent-optical-turns-10-Heres-how-it-was-made-prx.html

[5] S. Li *et al.*, "Enabling technology in high-baud-rate coherent optical communication systems," *IEEE Access*, vol. 8, pp. 111318–111329, Jun. 2020.

[6] S. L. I. Olsson, J. Cho, S. Chandrasekhar, X. Chen, E. C. Burrows, and P. J. Winzer, "Record-high 17.3-bit/s/Hz spectral efficiency transmission over 50 km using probabilistically shaped PDM 4096-QAM," in *Proc. Opt. Fiber Commun. Conf. Expo. (OFC)*, San Diego, CA USA,, 2018.

[7] M. Jinno, H. Takara, B. Kozicki, Y. Tsukishima, Y. Sone, and S. Matsuoka, "Spectrum-efficient and scalable elastic optical path network: Architecture, benefits and enabling technologies," *IEEE Commun. Mag.*, vol. 47, pp. 66–73, Nov. 2009.

[8] O. Gerstel, M. Jinno, A. Lord, and S. J. B. Yoo, "Elastic optical networking: A new dawn for the optical layer?" *IEEE Commun. Mag.*, vol. 50, pp. s12–s20, Feb. 2012.

[9] B. P. P. Kuo, E. Myslivets, V. Ataie, E. G. Temprana, N. Alic, and S. Radic, "Wideband parametric frequency comb as coherent optical carrier," *J. Lightw. Technol.*, vol. 31, pp. 3414–3419, Nov. 2013.

[10] M. Imran, P. M. Anandarajah, A. Kaszubowska-Anandarajah, N. Sambo, and L. Poti, "A survey of optical carrier generation techniques for terabit capacity elastic optical networks," *IEEE Commun. Surv. Tut.*, vol. 20, pp. 211–263, First quarter 2018.

[11] A. Rosado, A. Pérez-Serrano, J. M. G. Tijero, A. V. Gutierrez, L. Pesquera, and I. Esquivias, "Numerical and experimental analysis of optical frequency comb generation in gain-switched semiconductor lasers," *IEEE J. Quantum Electron.*, vol. 55, no. 6, pp. 1–12, Dec. 2019.

[12] R. Zhou, S. Latkowski, J. O'Carroll, R. Phelan, L. P. Barry, and P. Anandarajah, "40nm wavelength tunable gain-switched optical comb source," *Opt. Exp.*, vol. 19, pp. B415–B420, 2011.

[13] P. M. Anandarajah, S. P. Ó Dúill, R. Zhou, and L. P. Barry, "Enhanced optical comb generation by gain-switching a single-mode semiconductor laser close to its relaxation oscillation frequency," *IEEE J. Sel. Topics Quantum Electron.*, vol. 21, no. 6, pp. 592–600, Nov./Dec. 2015.

[14] A. Quirce *et al.*, "Nonlinear dynamics induced by optical injection in optical frequency combs generated by gain-switching of laser diodes," *IEEE Photon. J.*, vol. 12, no. 4, pp. 1–14, Aug. 2020.

[15] R. Zhou *et al.*, "Monolithically integrated 2-Section lasers for injection locked gain switched comb generation," *Opt. Fiber Commun. Conf.*, 2014, Paper Th3A.3.

[16] M. D. G. Pascual, V. Vujicic, J. Braddell, F. Smyth, P. M. Anandarajah, and L. P. Barry, "InP photonic integrated externally injected gain switched optical frequency comb," *Opt. Lett.*, vol. 42, pp. 555–558, 2017.

[17] P. M. Anandarajah *et al.*, "Flexible optical comb source for super channel systems," *OFC2013, OTh3I.8*.

[18] K. Iwashita and K. Nakagawa, "Suppression of mode partition noise by laser diode light injection," *IEEE J. Quantum Electron.*, vol. 18, pp. 1669–1674, Oct. 1982.

[19] E. K. Lau, L. J. Wong, and M. C. Wu, "Enhanced modulation characteristics of optical injection-locked lasers: A tutorial," *IEEE J. Sel. Topics Quantum Electron.*, vol. 15, pp. 618–633, May 2009.
[20] A. Murakami, K. Kawashima, and K. Atsuki, "Cavity resonance shift and bandwidth enhancement in semiconductor lasers with strong light injection," *IEEE J. Quantum Electron.*, vol. 39, pp. 1196–1204, Oct. 2003.
[21] N. Schunk and K. Petermann, "Noise analysis of injection-locked semiconductor injection lasers," *IEEE J. Quantum Electron.*, vol. 22, pp. 642–650, May 1986.
[22] P. Spano, S. Piazzolla, and M. Tamburrini, "Frequency and intensity noise in injection locked semiconductor lasers: Theory and experiments," *IEEE J. Quantum Electron.*, vol. 22, pp. 427–435, Mar. 1986.
[23] R. Lang, "Injection locking properties of a semiconductor laser," *IEEE J. Quantum Electron.*, vol. 18, pp. 976–983, Jun. 1982.
[24] F. Mogensen, H. Olesen, and G. Jacobsen, "Locking conditions and stability properties for a semiconductor laser with external light injection," *IEEE J. Quantum Electron.*, vol. 21, pp. 784–793, Jul. 1985.
[25] L. Li, "Static and dynamic properties of injection-locked semiconductor lasers," *IEEE J. Quantum Electron.*, vol. 30, pp. 1701–1708, Aug. 1994.
[26] T. B. Simpson, S. Wieczorek, B. Krauskopf, and D. Lenstra, "Mapping the complex dynamics of a semiconductor laser subject to optical injection," *AIP Conf. Proc.*, vol. 676, no. 1, pp. 375–375, 2003.
[27] T. B. Simpson, J. M. Liu, A. Gavrielides, V. Kovanis, and P. M. Alsing, "Perioddoubling route to chaos in a semiconductor laser subject to optical injection," *Appl. Phys. Lett.*, vol. 64, no. 26, pp. 3539–3541, 1994.
[28] V. Annovazzi-Lodi, S. Donati, and M. Manna, "Chaos and locking in a semiconductor laser due to external injection," *IEEE J. Quantum Electron.*, vol. 30, pp. 1537–1541, Jul. 1994.
[29] C. H. Lin and F. Y. Lin, "Four-wave mixing analysis on injection-locked quantum dot semiconductor lasers," *Opt. Exp.*, vol. 21, pp. 21242–21253, Sep. 2013.
[30] T. N. Huynh, L. Nguyen, and L. P. Barry, "Phase noise characterization of SGDBR lasers using phase modulation detection method with delayed self-heterodyne measurements," *J. Lightw. Technol.*, vol. 31, pp. 1300–1308, Apr. 2013.
[31] K. Kikuchi, "Characterization of semiconductor-laser phase noise and estimation of bit-error rate performance with low-speed offline digital coherent receivers," *Opt. Exp.*, vol. 20, pp. 5291–5302, Feb. 2012.
[32] J. Wang, M. K. Haldar, L. Li, and F. V. C. Mendis, "Enhancement of modulation bandwidth of laser diodes by injection locking," *IEEE Photon. Technol. Lett.*, vol. 8, pp. 34–36, Jan. 1996.
[33] X. J. Meng, T. Chau, and M. C. Wu, "Experimental demonstration of modulation bandwidth enhancement in distributed feedback lasers with external light injection," *Electron. Lett.*, vol. 34, pp. 2031–2032, Oct. 1998.
[34] Z. Liu and R. Slavík, "Optical injection locking: From principle to applications," *J. Lightw. Technol.*, vol. 38, no. 1, pp. 43–59, Jan. 2020.
[35] R. Zhou, T. N. Huynh, V. Vujicic, P. M. Anandarajah, and L. P. Barry, "Phase noise analysis of injected gain switched comb source for coherent communications," *Opt. Exp.*, vol. 22, pp. 8120–8125, Apr. 2014.
[36] K. Kikuchi, T. Okoshi, M. Nagamatsu, and N. Henmi, "Degradation of bit-error rate in coherent optical communications due to spectral spread of the transmitter and the local oscillator," *J. Lightw. Technol.*, vol. 2, no. 6, pp. 1024–1033, Dec. 1984.
[37] S. P. Ó Dúill, R. Zhou, P. M. Anandarajah, and L. P. Barry, "Analytical approach to assess the impact of Pulse-to-Pulse phase coherence of optical frequency combs," *IEEE J. Quantum Electron.*, vol. 51, no. 11, pp. 1–8, Nov. 2015.

Gaurav Jain was born in Chhatarpur, India, in 1993. He received the B.Tech. degree in electrical engineering from the Indian Institute of Technology Patna, Patna, India, in 2015, and the industrial-based Ph.D. degree from Pilot Photonics Ltd. and Trinity College Dublin, Dublin, Ireland, in 2020, which was funded by Irish Research Council. There he worked on the research and development of unique optical transmitters for high performance and energy efficient optical networks. Since 2020, he has been the Research and Development Manager of Pilot Photonics.

Deseada Gutierrez-Pascual received the B.Eng. degree in information technology from the Mikkeli University of Applied Sciences, Mikkeli, Finland, and the B.Eng. and M.Eng. degrees in telecommunications engineering from the University of Malaga, Málaga, Spain, and the industry-based Ph.D. degree from Dublin City University, Dublin, Ireland, in 2017. After M.Eng. degree, he joined Pilot Photonics Ltd., where she was a Senior Research Optical Engineer in an industry-based Ph.D. with Dublin City University, and funded by Irish Research Council, in the research and development of unique optical transmitters for high performance optical networks. Since 2017, he has been the Product Development Manager for Pilot Photonics.

Michael J. Wallace, biography not available at the time of publication.

John F. Donegan (Senior Member, IEEE) received the B.Sc. and Ph.D. degrees in physics from the National University of Ireland, Galway, Ireland. He was a Postdoctoral with Lehigh University, Bethlehem, PA, USA, and the Max Planck Institute, Stuttgart, Germany. He is currently a Professor of physics with the Trinity College Dublin, Dublin, Ireland, where he is also a Principal Investigator with the CRANN, AMBER, and CONNECT Research Centre. His current research interests include photonic structures, including broadly tunable lasers based on high order grating structures, plasmonic structures, light scattering in 2-D materials, and from planar structures. He is a Member of the American Physical Society and a Fellow of the Institute of Physics.

Prince Anandarajah (Senior Member, IEEE) received the B.Eng. degree in electronic engineering from the University of Nigeria, Nsukka, Nigeria, in 1992, the M.Eng. degree from Dublin City University (DCU), Dublin, Ireland, in 1998, and the Ph.D. degree from the Radio and Optical Communications Group, DCU, in 2003. He was an Instructor/Maintenance Engineer with the Nigerian College of Aviation Technology. He was also a Research Fellow and Research Officer until 2007, when he was appointed as a Senior Research Fellow. He is currently a Lecturer with the School of Electronic Engineering, DCU, a Principal Investigator for Science Foundation Ireland and Enterprise Ireland, and the Director of the Photonics Systems and Sensing Laboratory. He has authored or coauthored more than 240 articles in internationally peer reviewed journals and conferences, and is also a holder of six international patents, two of which have been licensed by industry. His main research interests include elastic optical networks, photonic sensing, spectrally efficient modulation formats, and radio-over-fibre distribution systems. He is also the Founder and Director of Pilot Photonics (a spin-off company).